IMPLEMENTING MULTI-SCALE AGRICULTURAL INDICATORS EXPLOITING SENTINELS

ATBD FOR CROP MAPPING ALONG THE SEASON WITH SENTINEL-1, -2 AND -3 IMAGES

ATBD CROP MAPS

ISSUE I2.00

EC Proposal Reference N° FP7-311766

Due date of deliverable: 2014-12-31

Actual submission date: 2016-04-29

Start date of project: 01.11.2012   Duration : 40 months

Name of lead partner for this deliverable: UCL

Book Captain: François Waldner

Contributing Authors: Pierre Defourny

Project co-funded by the European Commission within the Seventh Framework Program (2007-2013)		
Dissemination Level		
PU	Public	**X**
PP	Restricted to other programme participants (including the Commission Services)	
RE	Restricted to a group specified by the consortium (including the Commission Services)	
CO	Confidential, only for members of the consortium (including the Commission Services)	

DOCUMENT RELEASE SHEET

Book Captain:	François Waldner	Date: 29.04.2016	Sign.
Approval:	R. Lacaze	Date: 24.05.2016	Sign.
Endorsement:	M. Koleva	Date:	Sign.
Distribution:	Public		

CHANGE RECORD

Issue/Revision	Date	Page(s)	Description of Change	Release
	31/01/14	35	First Draft focusing on Russia study site	D1.00
D1.00	8/12/14	46	First Issue, including South-Africa study site	I1.00
I1.00	29/04/16	46	Updated for South Africa	I2.00

TABLE OF CONTENTS

LIST OF FIGURES

LIST OF TABLES

ACRONYMS

ATBD	Algorithm theoretical based document
CCI	Climate change Initiative
CE	Commission error
CGL	Crop group layer
CITARS	Crop Identification Technology assessment For Remote Sensing
CTL	Crop type layer
GIAM	Global irrigated area map
GMRCA	Global map of rainfed cropland areas
HRO	High resolution optical
LAI	Leaf area index
MODIS	Moderate Resolution Imaging Spectroradiometer
MRO	Moderate resolution optical
MSAVI2	Modified Soil Adjusted Vegetation Index
NDVI	Normalized Difference Vegetation Index
OE	Omission error
PCL	Pre-seasonal cropland layer

1. BACKGROUND OF THE DOCUMENT

1.1. EXECUTIVE SUMMARY

This ATBD (Algorithm Theoretical Based Document) describes the proposed algorithm for the production of crop maps along the season combining Sentinel-1, -2 and -3 proxy images with justification of the choices made. The objective assigned is to derive reliable (accuracy target set at 85%) crop maps as soon in the season as possible capitalizing on the advantage of each sensor: the temporal coverage of Sentinel-3, the high resolution of Sentinel-2 and the weather independent acquisitions of Sentinel-1. The output maps would support within season crop specific biophysical variable retrieval and area estimation.

The product consists in three different layers: (1) a cropland mask delivered at the beginning of the growing season, (2) a crop group map delivered at the end of the winter and (3) a crop type map updated along the growing season. The method has been developed and validated on two large sites to simulate Sentinel-2 wide swath: the Tula oblast in Russia (25 700km²) and the Free State province in South Africa (129 825km²).

1.2. SCOPE AND OBJECTIVES

One of the objectives of the ImagineS project is to improve the timing and the reliability of crop maps, either by integrating biophysical variables (see ATBD of FAPAR per crop and crop area) in the classification or combining multiple data sources. Those within season crop type masks are required to improve both crop acreage and yield estimates that in turn will provide production forecasts, amongst other applications.

More specifically, the Crop Mapping work package aims at providing sound basis for answering two research questions. First, it seeks to develop a methodology that combines the advantages of the 3 first sensor of the Sentinel programme: the temporal coverage of Sentinel-3, the high resolution of Sentinel-2 and the weather independent acquisitions of Sentinel-1. Indeed, reducing sensor dependence supports operational crop monitoring, e.g. in the event of sensor malfunctioning or frequent cloud occurrence. To that aim, the cropland description is updated along the season with an increased precision (increased number of classes and decreased omission and commission errors). The quantitative accuracy objective was set at 85%, as suggested by De Wit & Clevers (2004). The second objective is to assess how the large swath of Sentinel-2 could affect the classification. Indeed, vegetation gradient will occur within the same scene and could reduce the accuracy. If proven sensitive, the aim is also to propose method to mitigate this effect.

The objective of this document is to provide a detailed description and justification of the algorithm proposed. It should be noted that, at the time of the writing, access to field data over South Africa is being negotiated. Therefore, the results shown at the moment are valid for the Russian site and for South Africa when field data are not mandatory. When those field

data will become available, the full chain will be tested and evaluated. As the final version of the algorithm depends on the results that will be obtained for the South African site, the method might be updated accordingly if necessary.

1.3. CONTENT OF THE DOCUMENT

This ATBD document is split in 3 main sections:

1. **Algorithms overview.** This section contains:
   a. A definition of the proposed products;
   b. A brief description of the sensors used and the pre-processing of their images;
   c. The outline of the algorithms.
2. **Description of the Algorithms.** This section contains:
   a. The inputs required and the outputs provided by the algorithms;
   b. The classification technique. Three sensor specific classifiers are trained and their outputs are merged for the final classification.
3. **Quality assessment.** This section contains accuracy assessments of the three products for the growing season of 2013 in Russia, and of the two first products for South Africa

1.4. RELATED DOCUMENTS

1.4.1. Inputs

Overview of former deliverables acting as inputs to this document.

Document ID	Descriptor
ImagineS_RP1.1_URD	Users Requirements Document
ImagineS_RP1.2_SSD	Service Specifications Document

1.4.2. Output

Overview of other deliverables for which this document is an input:

Document ID	Descriptor
ImagineS_D4.2	Crop maps products
ImagineS_RP6.3_PUM_CropMaps	Product User Manual of the crop maps products

2. OVERVIEW

2.1. STATE OF THE ART

Recent and forthcoming development of satellite remote sensing offers many possibilities for mapping cropland and crop types in various agricultural landscapes. A large diversity of cropland mapping strategies at different scales associated with various degrees of accuracy can be found in the literature.

From local to regional scale, croplands are often depicted according to land cover typology focusing mainly on the natural vegetation types. Crop lands are often included in mosaic or mixed classes making them difficult to use for agricultural applications (neither as agricultural mask, nor as a source for area estimates).This is typical for global land cover products, such as GLC2000 (Bartholomé and Belward, 2005), GlobCover 2005/2009 (Defourny et al. 2009, Bontemps et al. 2010), GLCShare, MODIS Land Cover (Friedl et al., 2002), which are not specifically targeting the agriculture component of the landscape. Even the most recent and more precise ESA Climate Change Initiative (CCI) Land Cover products obtained from a multi-year multi-sensor approach still consider the croplands as any other land cover classes (Bontemps et al., 2012). Alternatively, a few global crop maps were produced at global and continental scale. Pittman et al. (2010) produced the map of global cropland extent at 250 m spatial resolution using multi-year MODIS data and thermal data. Two other global maps specifically dedicated to croplands were produced with an emphasis on water management: the global map of rainfed cropland areas (GMRCA) (Biradar et al., 2009) and the global irrigated area map (GIAM) (Thenkabail et al., 2009). However, their coarse spatial resolution (10 km) does not meet the needs for operational applications and suffer from large uncertainties (Portmann et al., 2000) – especially in complex farming systems in Africa. Several initiatives adopted existing land cover products as inputs. Ramankutty et al. (2008) combined two satellite-derived land cover maps (Boston University's MODIS-derived land cover product (Friedl et al., 2002) and the Global Land Cover 2000 (GLC2000) data set (Mayaux et al., 2004)) with an agricultural inventory to produce the cropland mask at 10 km. One alternative for better cropland information is through hybridization, e.g. the integration of all available maps into a single product (RD.174). In that vein, Fritz et al. (2011) combined existing land use/land cover data sets (i.e., GLC2000, MODIS Land Cover, and GlobCover relying on expert knowledge and national statistics to produce a probability map of cropland areas. However, the product merges general land cover products that do not focus on agricultural areas and that have an unadapted spatial resolution for mapping cropland (from 300 m to 1 km). To cope with these issues, Vancutsem et al. (2013) compared and combined ten data sets through an expert-based approach in order to create the derived map of cropland areas at 250 m covering the whole of African continent. Still at the regional scale, RD.28 proposed a dynamic mapping of cropland areas in Sub-Saharan Africa using MODIS time series. Yet, these compilation efforts, while being extremely valuable, present the two-fold disadvantage of being spatially inconsistent and out-of-date.

More recently, large scale remote sensing product have been completed to deliver a global croplands mask (Pittman et al., 2010) or a global soybean distribution map (Hansen et al., 2012 – oral communication). At the national level, Thenkabail and Wu (2012) developed an automated cropland classification algorithm combining Landsat, MODIS, and secondary data to differentiate cropland extent, areas, and characteristics (e.g., irrigated vs. rainfed). Besides, Vintrou et al. (2012) proposed a stratified approach to discriminate the cultivated areas in the fragmented rural landscapes of Mali. Locally, cropland is often extracted in a two-step classification scheme to support further crop type distinction (Shao et al., 2010; Arvor et al, 2011). Crop inventory by remote sensing has been studied extensively since the early days of the discipline. CITARS (Crop Identification Technology assessment For Remote Sensing) was features in the same classification algorithm and demonstrated its relevance for crop type classification. Another aspect, independent from the classification algorithm, is related to the considered spatial unit, which can be either the pixel or the field. Pixel-based classification techniques often failed to determine the borders of agriculture parcels (Ormeci, 2010). Spatial filters increase the accuracy by removing the small inclusions of other classes within the dominant class (Yang et al., 2007). Parcel-based approach was found to be more accurate than pixel-based (Ozdarici et al., 2012). Field limits might be derived either from digital vector database (De Wit, A. J. W. and Clevers, 2004) or by segmentation (Castillejo-Gonzalez et al., 2009). Even if Sentinel-2 spatial resolution is expected to resolve most fields, it seems that in particular conditions (Delrue et al., 2013) sub-pixel approaches (as developed by Lobell and Asner, 2004; Ozdogan, 2010 and Atzberger and Rembold, 2012) will remain necessary.

Similarly, many methods have been devised to extract crop cover from radar imagery either directly to the backscattering coefficients (Del Frate et al., 2003) or to extracted features such as texture indices (Yang et al., 2010), polarimetric features (Cloude and Pottier, 1996) or color features (Uhlmann and Kiranyaz, 2014). Some of these radar-specific feature required dedicated algorithm for classification such as Wishart maximum likelihood classifier (Lee et al., 2001; Skriver et al., 2011, Ainsworth et al. 2009), fuzzy- (Chen and Chen, 2003), and complex-valued neural network (Hänsch, 2010). Of course, some research studies also worked on a combination of SAR and high resolution (Blaes et al., 2005) or high and moderate resolution (Thenkabail and Wu, 2012).

To date most experiments looked at crop classification from an end of season point of view, selecting the best-suited band/date combination to maximize the classification accuracy. Early mapping along the growing season represent a major challenge as only incomplete growing season time-series information is available (Kastens et al, 2005). In such a context, reducing dependence on one sensor would support operational crop monitoring as sensor malfunction and cloud coverage at critical periods might jeopardize the accuracy requirements of the map (McNairn et al., 2009).

The method proposed in this ATBD combines three different kinds of sensor and might be extended to more which reduces the sensor dependence and enhances the probability of

acquiring during a good discrimination window. Besides, this combination makes the classification method more robust to address the large spectrum of agro-system.

2.2. THE CONSIDERED PRODUCTS

The considered product corresponds to three layers of crop maps with an increasing level of details in both the legend definition and the spatial resolution as information – and thus potential class separability windows– accumulates along the season. Such products are delivered per growing season, typically one or two growing cycle for the rainfed agriculture, and possibly more for the irrigated lands.

2.2.1. Pre-seasonal cropland layer

The pre-seasonal cropland layer (PCL) corresponds to the most up-to-date cropland map extent for a defined cropping season. Existing land cover information is updated based on the previous year to provide most current extent of the cropland according to a change detection approach. The pre-seasonal cropland layer distinguishes two classes: cropland – which is defined by the annually planted land – and non-cropland.

2.2.2. Crop group layer

The crop group layer (CGL) aims at further discriminating the cropland between winter crops and other crops which include spring crops but also fallow. Winter crops are of two kinds: 1) those sown before or during the winter time and that need cold temperatures to grow in the spring/summer (e.g. winter wheat in Russia) and 2) those having a full development cycle (e.g. winter wheat in South Africa). The recognition method of winter crops follows an automated time-series analysis approach based on the detection of an increase in the vegetation index during the winter. To ensure consistency between the products, crop groups can only occur within the cropland.

2.2.3. Crop type layer

The crop type layer (CTL) gives the most detailed picture of the cropland distinguishing the dominant crop types of a given region. Thus, the legend depends on the presence/absence of particular crops in the region of interest recognized thanks to a machine learning approach. This concerns only mono-specific agricultural fields.

2.3. INSTRUMENTS' CHARACTERISTICS AND DERIVED DATA

As the objective is to develop a method for Sentinel-1, -2 and -3 which are not yet operational, the method has been developed and tested on the following proxies: Radarsat-2

for Sentinel-1, RapidEye for Sentinel-2 and MODIS for Sentinel-3 (see Tab.1 for a comparison). These proxies have been chosen in order to match as closely as possible the specifications of the Sentinel sensors.

Table 1: Comparison of the Sentinel sensors and their respective proxy for the Russian site

	SENTINEL-1	RADARSAT-2	SENTINEL-2	RAPIDEYE	SENTINEL-3	MODIS
Nominal Swath	80-km	300-km	290-km	77-km	1250-km	2330-km
Wavelength (μm)/frequency	C-band	C-band	blue (0.42-0.55), green (0.53-0.59), red (0.63-0.69), red-edge (0.69-0.72, 0.72-0.75, 0.76-0.8, 0.84-0.89), near-infrared (0.72-0.96) and 5 others	blue (0.40-0.51), green (0.52-0.59), red(0.63-0.685), red-edge (0.69-0.73), near-infrared (0.76-0.85)	red (0.6-0.7), near-infrared (0.88-0.89) and 19 others	red (0.62-0.67), near-infrared (0.84-0.88) and 34 others
Polarization	HH+HV VV+VH	HH+HV VV+VH	NA	NA	NA	NA
Beam Incidence angle	20°-41°	20°-46°	NA	NA	NA	NA
Ground resolution	5-m	25-m	10-m	5-m	300-m	250-m
Repeat cycle	2 days using a constellation of satellites	programmable	5 days with a pair	daily with 5 satellites	1-2days with a pair	1-2 days

Instead of Sentinel-1 images, Radarsat-2 ScanSar Narrow or Radarsat-2 Wide Fine images were acquired in dual polarization VV-VH, for Russia and South Africa respectively. Images were multi-looked, ortho-rectified, radiometrically calibrated and co-registered. A 9x9 enhanced Frost filter was applied to reduce the speckle.

RapidEye high resolution optical (HRO) time-series served as proxy for Sentinel-2. The images were ortho-rectified and the observations were converted from digital numbers to top-of-atmosphere reflectance. The *unusable data mask* provided along with the images, even though perfectible, masked out the clouds. In case of large cloud contamination, tiles were acquired multiple times within the same acquisition window. Data gaps of the less contaminated images were partially or totally filled combining the overlaying additional observations within the same acquisition window. This maximizes the homogeneity of the resulting images. To match the spatial resolution of Sentinel-2, images were re-sampled at 10-m using a nearest neighbor approach.

MODIS data simulated the medium resolution optical (MRO) time-series Sentinel-3. From daily quality controlled reflectance values of Terra and Aqua, 10-day mean composites were produced according to the procedure developed by Vancutsem et al. (2007). Because South

Africa had clearer sky conditions, it was possible to reduce the compositing window to seven days, allowing a closer monitoring of the vegetation. The mean compositing reduces the bidirectional reflectance distribution function and atmospheric artifacts, produces spatially homogeneous cloud-masked composites with good radiometric consistency and does not requiring model adjustment or additional parameterization. A soil adjusted vegetation index with a self- adjusting soil brightness correction factor, the MSAVI2 (Qi, Chehbouni, Huete, & Kerr, 1994), was calculated for every pixel of the image as follows:

$$MSAVI2 = \frac{(2\rho nir + 1) - \sqrt{(2\rho nir + 1)^2 - 8(\rho nir - \rho red)^2}}{2}$$

where ρnir and ρred are reflectances in the near infrared and red band, respectively. Time-series were then smoothed and gap filled with the Whittaker filter (Eilers, 2003). The gap filling ability of this filter is particularly interesting in cloud persistent areas.

Given the correlation between vegetation indices and biophysical variables such as the Leaf Area Index (LAI), it is to be emphasized here that the MSAVI2 could be replaced by biophysical variables. However, due to the insufficient spatial resolution of the current global products (1-km), this is not yet implemented. Since it is planned in ImagineS to provide bio-physical variables at 300-m, this approach would be tested when the products are made available.

2.4. DEVELOPMENT AND TEST SITES

The algorithm proposed in this ATBD has been tested over the two study sites with proxies for Sentinel data. One image acquisition campaign was planned per study site (Fig. 1). For the growing season of 2013 in Russia, eleven Radarsat-2 images and 5 RapidEye coverages were acquired from February to August (Fig. 2). MODIS acquisitions span from January 2012 to August 2013. For the growing season of 2014 in South Africa, 12 Radarsat-2 images and RapidEye coverages were acquired from August to April (Fig. 3). MODIS acquisitions span from August 2012 to April 2014.

Figure 1: Location of the South African site and the Russia study site.
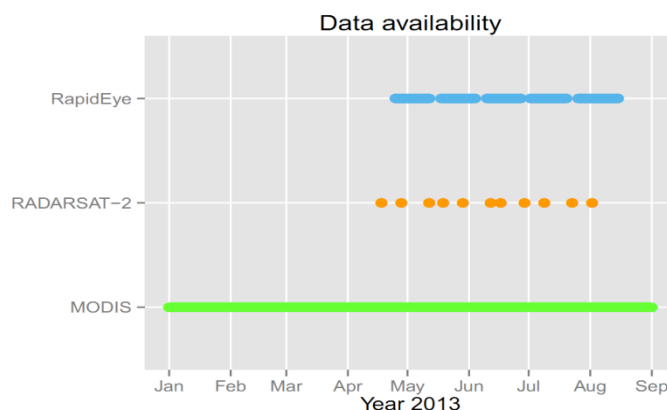
Figure 2: Data acquisition for the Russian site
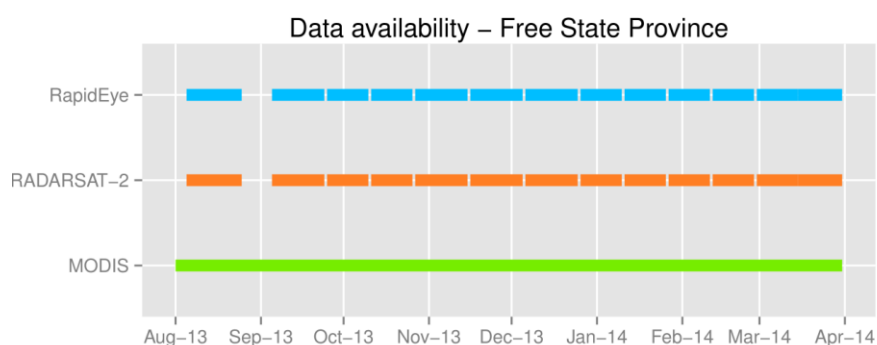
Figure 3: Data acquisition for the South-African site

2.5. REQUIREMENTS FOR THE ALGORITHM SELECTION AND DESIGN

The objective is to develop an algorithm dedicated to multi-sensor crop discrimination along the season. The classification framework seeks to achieve the best accuracy regionally on the test site while ensuring a good performance over other untested agro-systems. The method should also be flexible and adaptable to ingest different data sources –such as Landsat-8– and ensure consistency between the products. Depending on the layer to be produced, the algorithm would run at the pixel or at the object level.

The pre-seasonal cropland layer and the crop group layer are mapped once a year, at the beginning of the season and at the end of the winter respectively, with a spatial resolution of 250-m (and possibly down to 10-m if high resolution images are available). The crop type layer, i.e. the end-of-season product, has the same spatial resolution as Sentinel-2. The crop type layer is updated along the growing season at each new high resolution image

2.6. ALGORITHM OUTLINE

The classification method combines the advantages of each satellite: the temporal coverage of Sentinel- 3, the high resolution of Sentinel-2 and the weather independent acquisitions of Sentinel-1. However, due to the mismatch between the start of the project and the start of the growing season (at least in Russia), the synergy between the three sensors will be fully exploited only during the second half of the season (e.g. after the winter). The algorithm produces three crop maps with an increased level of thematic and spatial details as information is ingested (Figure 4).
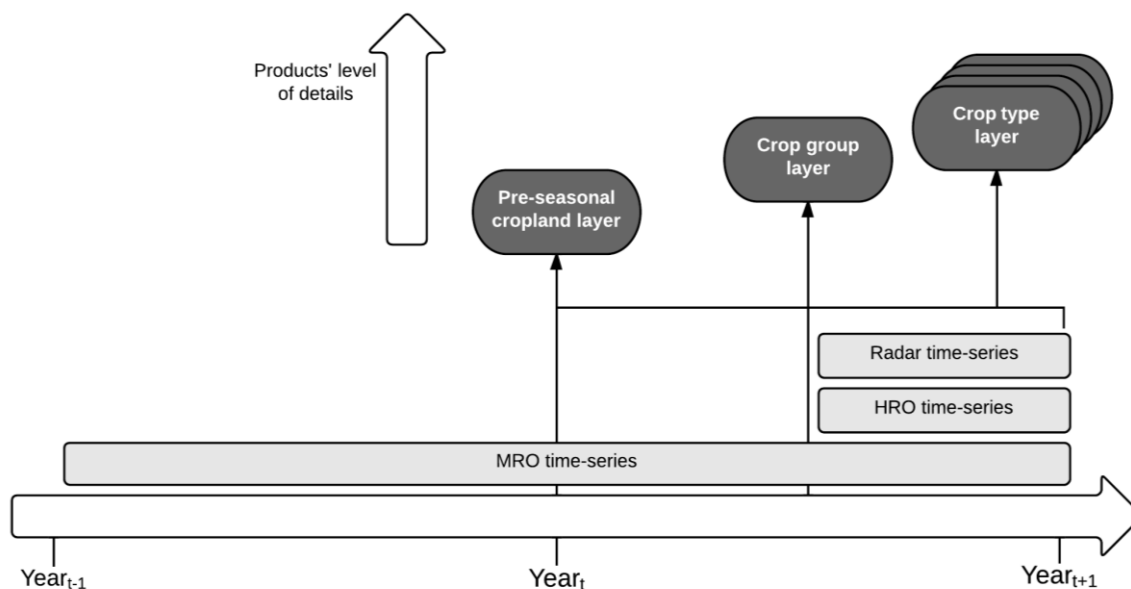
Figure 4: Timeline of the production of the crop maps.

At the beginning of the cropping season, a pre-seasonal cropland extent map is produced using a dedicated land cover change algorithm based on the previous year metrics at moderate resolution. The best local land cover map available helps this early diagnosis. If none is available, a global land cover map (such as GlobCover) is used. Since those land cover map do not target agricultural land and since changes may have occurred, an image-to-map discrepancy has been developed to adjust it to the current regional conditions.

At the end of the winter, a knowledge-based crop group layer distinguishing winter crops from summer crops is delivered thanks to an automated phenological object-based time-series classification of medium resolution data. A first step relies on a harmonic components analysis to spatially group pixels with the same temporal trajectories. As multi-date segmentation is known to perform better than single-date but requires the prior identification

of key-dates, segmenting on the harmonic components is an alternative to overcome this constraint. Second, the automated adaptive recognition decision rule relies on the presence or absence of an observable winter growth peak.

Along the growing season, a multi-sensor crop specific classification is finally achieved. The crop type layer is updated as data acquisition progresses, taking into account the agricultural calendar and the crop rotation systems. Crops type maps are produced through an iterative segmentation, classification and fusion scheme of the moderate and high resolution optical and radar images. The updates take place at each new acquisition of high resolution imagery.

3. ALGORITHM DESCRIPTION

In this section, the inputs and outputs are described. Then, the different steps of the algorithm are presented.

3.1. INPUTS

All these inputs are required for each considered pixel. For the sake of clarity considering the number of products, this section details only briefly the inputs. More details are provided at the beginning of each algorithm description.

3.1.1. Satellite data

The satellite data (radar, MRO and HRO) need to be pre-processed according to the procedure detailed in the sensor overview. MRO vegetation index time-series varies between -1 and 1. Radar units are expressed in terms of back-scattering coefficients in the VH and VV channels. HRO time-series are cloud free top-of-atmosphere reflectance data in the five bands of RapidEye. Missing data can still occur at that stage. All images have WGS84 as spatial coordinate system. For the crop type layer, a nearest neighbor re-sampling to the RapidEye grid degraded at 10-m is needed.

3.1.2. Land cover map and training data

The best available land cover map is necessary as training data for the pre-seasonal cropland layer. In addition, field data is required for the training of the crop type layer classifiers. This field data set consists in field level observations of crop types for which the temporal profiles have been extracted. Besides, observations of other non-agricultural land cover types have been added to the data set by means of visual interpretation on Google Earth and using existing land cover maps.

3.2. OUTPUTS

For each product, the outputs will be provided by application of the algorithm over each time-series. Each product is a single-band raster accompanied by its legend. The resolution of each product varies according to the data input (Table 2).

Table 2: Products description

Product Name	Temporal resolution	Spatial resolution	Thematic resolution
Pre-seasonal Cropland Layer	Once a year, beginning of the season	250-m	Cropland, Non-cropland
Crop Group Layer	Once a year, end of the winter	250-m/10m	Winter crop, other crops
Crop Type Layer	Every 15 days, along the spring and summer	10-m	Crop types, depending on the area of interest

3.3.   ALGORITHM DESCRIPTION

3.3.1.   Pre-seasonal Cropland Layer (PCL)

INPUTS	• Seven or Ten-day mean composite time-series of moderate resolution vegetation index from the previous year [start of season year t-1 $\rightarrow$ start of season year t] • Re-sampled and co-registered land cover map

The core of the method relies on a change detection method called normal iterative trimming (Fig. 5). Iterative trimming is a change detection technique that identifies outliers as plausible candidates for change (Desclée, Bogaert, & Defourny, 2006) and can be used to automate image-to-map discrepancy detection (Radoux, 2010). To identify candidate pixels for land cover change between the available map and the time-series (that is the outliers that need to be reclassify), a multivariate normal iterative trimming was chosen.   The classification considers four time-series features (mean, maximum, minimum, slope between the minimum and the maximum) that were extracted from the time-series themselves.

First, all the mixed classes were considered as outliers and set aside. Second, for each of the remaining land cover class, the selection of outliers relied on a probability threshold α which specifies the limit at which an observation is considered an outlier. The distribution is iteratively trimmed until no more outliers are identified. For the normal case, the outlier detection criterion gives:

$$(x - \mu)'\Sigma^{-1}(x - \mu) \leq \chi_p^2(\alpha)$$

where χ^2 is the upper $(100\alpha)^{th}$ percentile of a χ_p^2 distribution with *p* degrees of freedom. The threshold α was set at 0.05. The multivariate normal iterative trimming is applied on each pure thematic of the reference land cover map except the mosaic classes. The outliers were merged to the mosaic class' pixels and are subsequently reclassified according to a maximum likelihood decision rule. The output classes are defined by the parameters of the trimmed classes. A priori probabilities were computed from the initial land cover map with mixed classes probabilities redistributed to the closest thematic class. The four metrics were scaled and centered to avoid confusion between different metric units. The updated land

cover map details as many classes as pure classes in the initial legend. Non-crop classes are finally grouped in order to focus the classification on cropland detection.
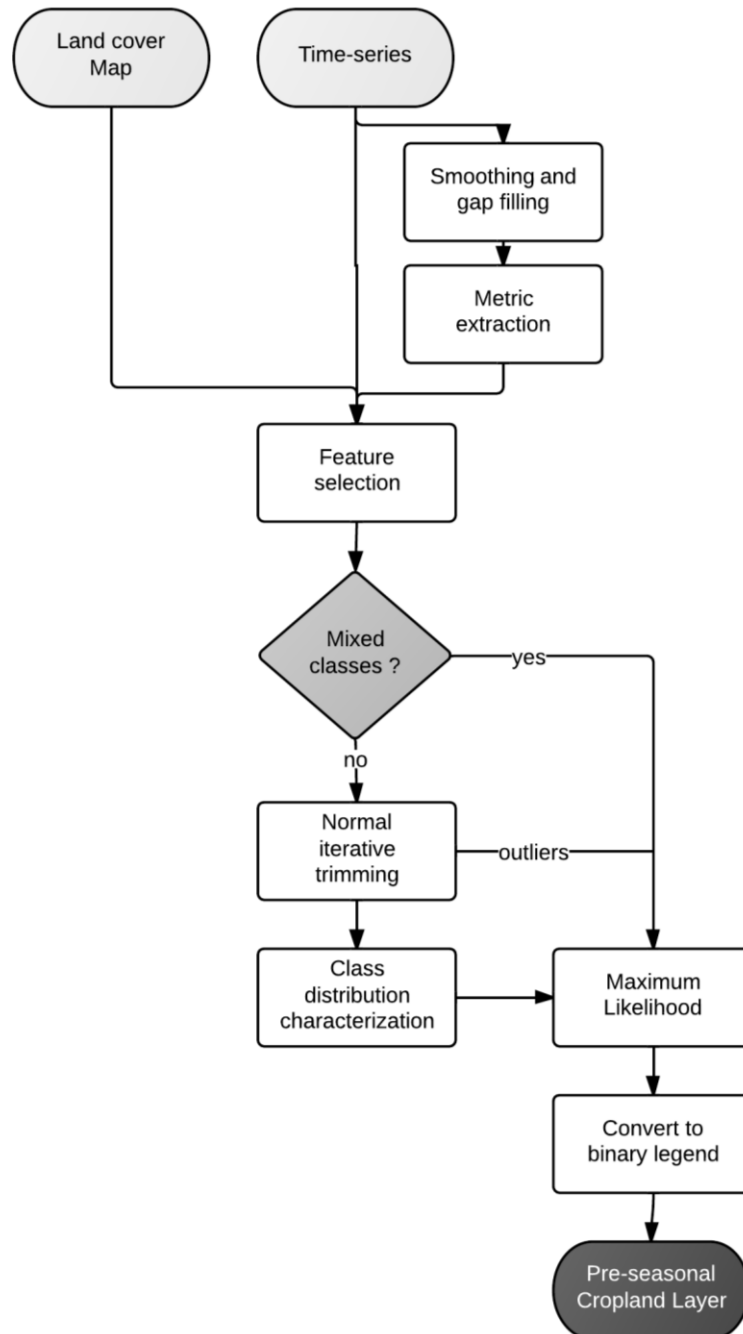
Figure 5: Flowchart of the pre-seasonal cropland layer

3.3.2. Crop Group Layer (CGL)

Two algorithms are proposed to produce the crop group layer because the sites have different winter growing conditions. From an agronomic point of view, winter crops in Russia characterize crop that need to be exposed to low temperatures (vernalization) in order to complete their vegetative cycle whereas winter crops in South Africa complete their vegetative cycle before in the spring. Second, no high resolution image was available for Russia in the winter period which was not the case for South Africa. To include those high resolution images in the winter crop detection algorithm, some modifications were mandatory. It should be noted here that including high resolution images was not the main driver of this choice because the same modifications are also applicable in Russia.

Apart from these differences, the rationale behind the detection algorithm is fundamentally the same: exploit the part of the signal particular of winter crops, i.e. an increase of the vegetation index corresponding to crop development.

3.3.2.1. Winter crop detection in Russia

INPUTS	• Ten-day mean composite moderate resolution time-series of vegetation index from the previous year [01-07-year t-1 → 01-03-year t] • Pre-seasonal cropland layer

A two-step object-based classification addresses the binary classification of winter crops versus summer crops (Fig. 6). In the first step, objects are derived by means of a segmentation on the harmonic components of the time-series (Jakubauskas, Legates, & Kastens, 2002). In the second, an automated time-series analysis based on phenological metrics classifies the objects in the two classes. The previously derived cropland masks out the non-agricultural areas.

Figure 6: Flowchart of the crop group layer algorithm.
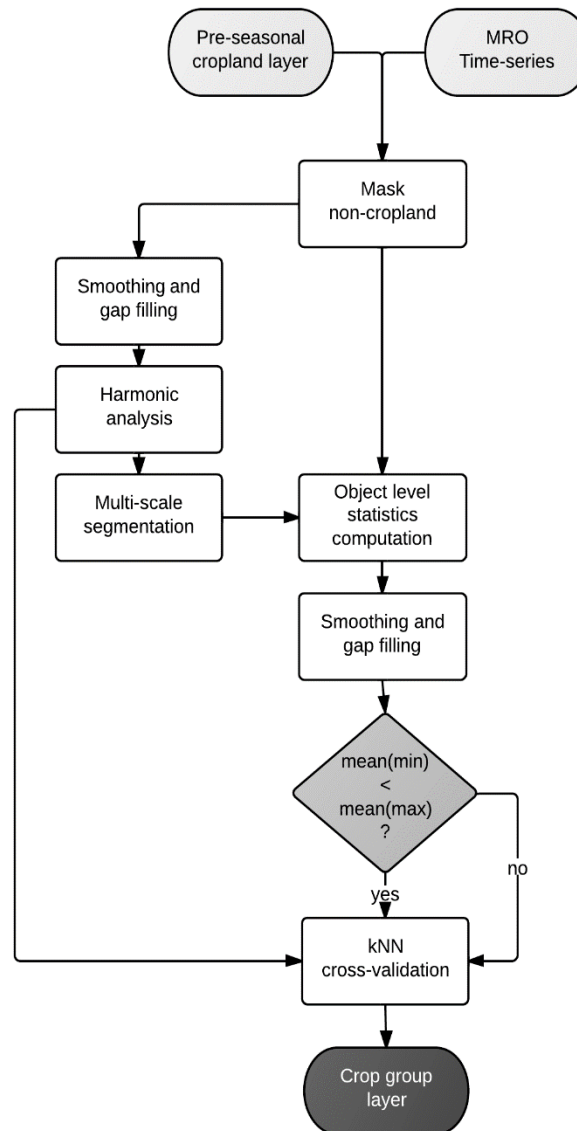
The harmonic analysis was applied pixel-wise. A Fourier transform converts the input time-series into a complex array with a real and an imaginary part. The real (a) and an imaginary (b) part can be converted to polar form. Each order i is defined by its phase φ_i and amplitude a_i:

$$a_i = \sqrt{a_i^2 + b_i^2}$$

$$\varphi_i = \arctan\frac{b_i}{a_i}$$

As the high orders contain mainly noise, only the additive term and the two first harmonic are kept. Similar pixels were then spatially grouped based on the similarity of the two first harmonic and the additive term using the multi-resolution segmentation algorithm (Baatz & Schäpe, 2000) (Fig. 7).

a)   b)   c)
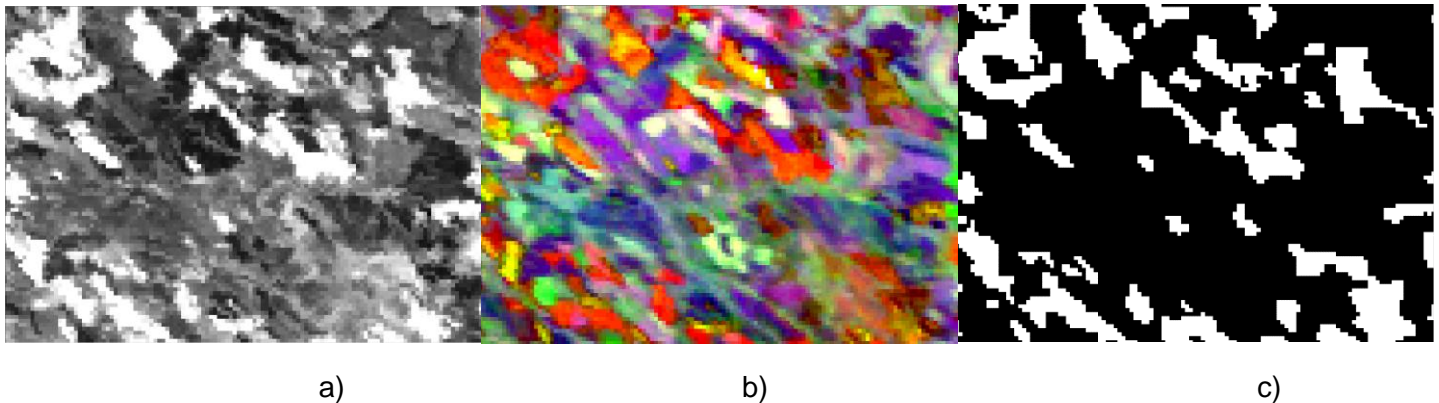
Figure 7: a) MSAVI2 (2013-11-10), bright colors are high MSAVI values; b) color composition (additive term, amplitude and phase of the first harmonic); c) crop group layer. The harmonic components catch the temporal trajectory of the pixels (winter crop in red) and are a reliable base for segmentation

The second step corresponds to the classification of the objects. A knowledge-based adaptive decision rule has been defined based on a specific temporal pattern of the winter crop: the presence of a winter growth peak (Fig. 8). For each object-level time-series, the algorithm extracts three metrics: (i) the snow date corresponds to the dekade during which the MSAVI2 signal falls below a threshold, (ii) the maximum of vegetation is the local maximum MSAVI2 value at the winter growth peak and (iii) the local minimum preceding the winter peak. The simplest decision rule would classify as winter crop every feature with a winter peak, but this hypothesis does not hold as other landscape elements also exhibit a maximum. Usually, those elements however are characterized by a rapid drop and then increase of the signal whereas winter crop shows a plateau corresponding to field preparation and sowing. To tighten the rule, the minimum and the maximum are converted into local average of the metric values: an object is classified as winter crop if $mean(max) > mean(min)$. This filters out objects without a significant increase in their respective trajectory.
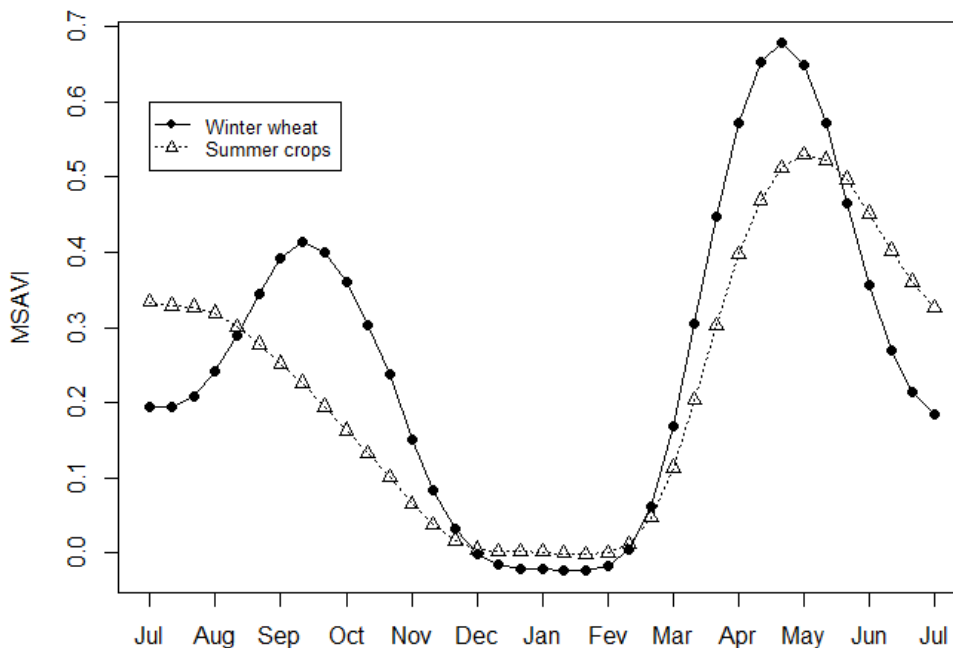
Figure 8: Average temporal profile for the dominant winter crop in Russia and the summer crops.

To strengthen the accuracy of the classification, a cross-validation based on the harmonic components is added. The 25-nearest (in Euclidean distance) vectors are identified and the final label is decided by majority vote. The harmonic component values are first standardized and then averaged per object

3.3.2.2. *Winter crop detection in South Africa*

INPUTS	• Seven-day mean composite moderate resolution time-series of vegetation index from the previous year [01-06-year t→ 01-11-year t] • RapidEye images until 01-11-year t • Radarsat-2 images until 01-11-year t • Pre-seasonal cropland layer

Holding to the same approach as for vernalizing areas, a three-step winter crop detection was designed combining an automated detection approach at moderate resolution with an object-oriented approach at high resolution.

First, the slope between the minimum and the maximumn was derived from the MSAVI2 MODIS time-series. Areas with positive values correspond to winter growing areas whereas slow decreasing values characterize, other land cover types such as winter grazing areas. Second, if using the slope appears as an efficient automated recognition method, the spatial resolution remained to low. To increase the spatial details, a segmentation was carried out

on the NDVI high resolution optical images. Average object-level statistics were then computed – mean σ_{VH}, σ_{VV}, NDVI and slope. Third, an unsupervised clustering was then applied locally (moving windows of 50x50-km) on sigma and NDVI. As setting the number of cluster is always a difficult task but of key importance, the local training allows to reduce the variability within the area to be classified. Clusters having 40% or more of their sample associated with a positive slope were labeled as winter crops. Refine the delineation of winter crop field but also include smaller fields for which the winter growth cycle was not picked up because of MODIS spatial resolution.
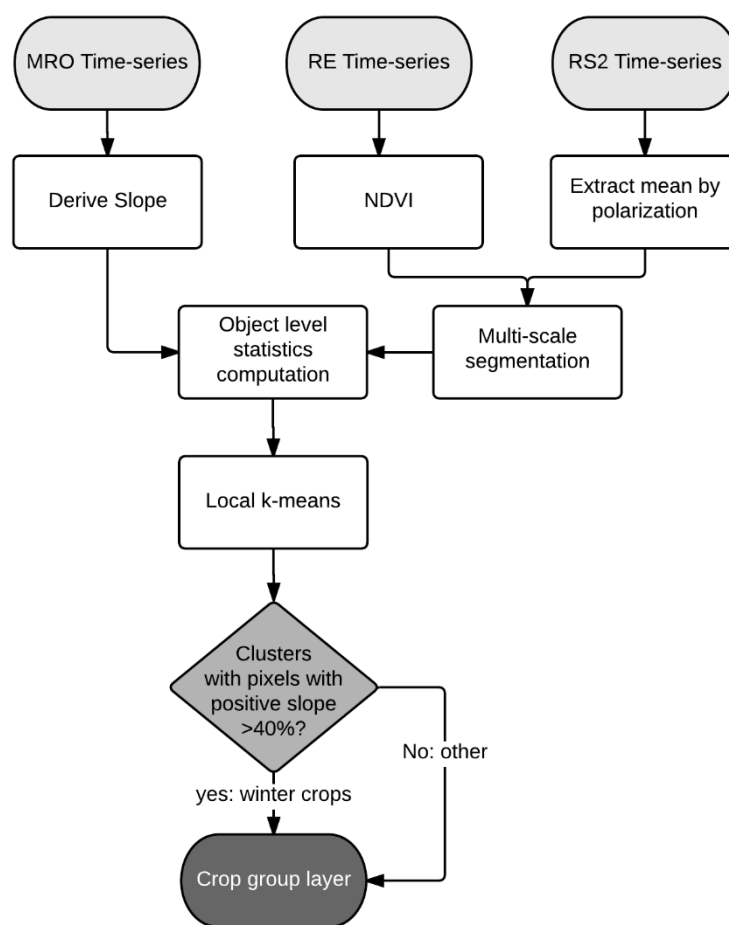
Figure 9: Flowchart for the winter crop classification with the Free State data set

3.3.3. Crop Type Layer (CTL)

INPUTS	• Seven or Ten day moderate resolution vegetation index time-series [01-07-year t-1 → harvest]
	• Preprocessed, re-sampled and co-registered radar data [start of spring - harvest]
	• Preprocessed, RapidEye data [start of spring - harvest]
	• Crop type field observations

Three different processing chains have been developed, one per sensor (Fig. 10). The only information shared is the spatial delimitation of the objects. Each sensor has its own classifiers and the resulting classifications are fused into the final classification.
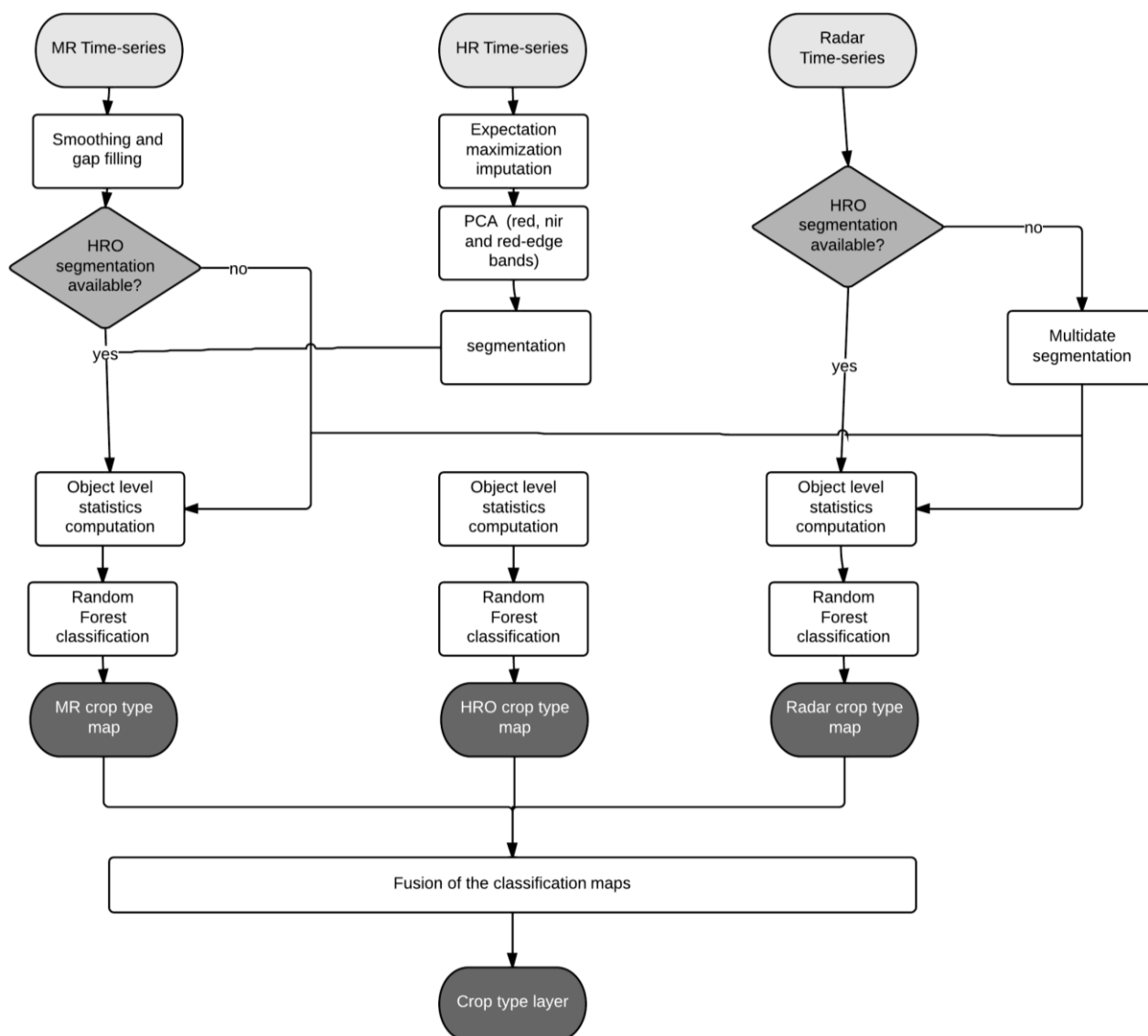

Figure 10: Flowchart of the crop type layer algorithm.

3.3.3.1. *Missing values and smoothing*

As classifiers cannot handle with missing observations, reconstruction of missing data is a mandatory step. MRO time-series are smoothed and gap-filled by means of the Whittaker

filter (Eilers, 2003). For HRO, due to the short length of the HRO time-series (only 5 coverages in Russia), traditional filters for filling the missing values were discarded. Instead, a temporal linear interpolation was run the incomplete HRO to impute them. At the first acquisition of HRO data imputation with linear interpolation is infeasible; missing data are thus imputed thanks to a weighted mean of the k-nearest neighbors identified with the radar data.

3.3.3.2. Segmentation

The Sentinel-2 like images is the primary source for segmentation because of their higher spatial resolution. The NDVI of each images were stacked and put into a principal component analysis that will reduce the dimension for the segmentation while maximizing the variance of the output components. A multi-resolution segmentation algorithm was then applied on the time stack of NDVI. Besides, if no HRO image is available at the acquisition of the first radar images, the segmentation is applied on the radar data only with its respective parameters.

3.3.3.3. Objects statistics computation

Object-level statistics are computed using the latest segmentation available. Only average values of the input data are computed, that is: the mean MSAVI2, σ_{VH}, σ_{VV}, and blue, green, red, infra-red and red-edge.

3.3.3.4. Training of the classifiers

At each acquisition of a high resolution data (either radar or optical), new classifiers are trained to include the new observations. One random forest with 800 trees is trained by data source: one for the MODIS data, one for the Radarsat-2 data and one for the RapidEye data. It should be that several classifiers have been tested and that the random forest was outperforming the others for every sensor. Random forests are insensitive to noise and overtraining (Breiman, 2001). Their internal selection of variables is expected to prevent from the side effects of high dimensionality.

3.3.3.5. Classification

At each acquisition of a HR image, the classifiers are applied per data type on all available images to produce three sensor-specific crop type maps.

3.3.3.6. Map fusion

Several strategies for map fusion have been developed such as the Dempster-Shafer theory (Hégarat-Mascle, Richard, & Ottlé, 2003). In this framework, the performance of each classifier resulting in the classification maps to fuse are evaluated with the help of a class-specific belief function which measures the degree of belief that the corresponding label is correctly assigned to a pixel. For each classifier, and for each class label, these belief functions are estimated from another parameter called the mass of belief of each class label,

which measures the confidence that the user can have in each classifier according to the resulting labels. The fused class label for each pixel is the one with the maximal belief function. In case of multiple class labels maximizing the belief functions, the output fused pixels are set to the undecided value. In that case, the labels from the most accurate individual map are kept.

As the availability of the training data might be a constraint and because the availability of calibration data might change from year to year, the approach chosen to fuse the results of the classifiers is rather based on their soft outputs, i.e., their class membership. The class membership is of the following form:

$$pr(x) = \{pr_1(x), pr_2(x), \dots, pr_i(x), \dots, pr_n(x)\}$$

where $pr_i(x)$ is the estimated membership degree of a object x to class i, and n the number of classes. The vectors pr_{MODIS} (x,) $pr_{RADARSAT}$ (x) and $pr_{RAPIDEYE}$ (x) for each object resulting from the three independent classifications are then multiplied class-wise and the class that maximizes the class membership is taken as the final output of the classification.

4. QUALITY ASSESSMENT

Confusion matrices as well as the overall accuracy, the producer's accuracy and the user's accuracy are the measures chosen to assess the products. The overall accuracy is the total classification accuracy. The producer's accuracy refers to the probability that a certain land-cover of an area on the ground is classified as such, while the user's accuracy refers to the probability that a pixel labeled as a certain land-cover class in the map is really this class.

For the Russian site, the accuracy of the three products was assessed thanks to the field data collected in July 2013 and an available vector layer delineating the field parcels. This vector layer of field boundaries were manually digitized on Landsat-5 and 7 images and last updated in 2012. The data set contains 600 punctual observations of 12 different agricultural dominated by winter wheat and spring barley. A parcel database is also available. Fields were manually digitized on Landsat-5 and 7 images and last updated in 2012. The punctual observations were converted in areal observations thanks to this database. An additional visual verification of the parcel boundaries was completed using the RapidEye images of the current year. In general, the quality of the data set is good but some fields have been discarded due to their inadequation between their label and their expected crop development calendar.

For the South African site, field data was derived from 1) cropland parcel information for the PCL and 2) two sets of ground truth samples collected in the framework of the Producer Independent Crop Estimate System. The field boundary data set has been manually digitized by visual interpretation on SPOT-5, -6 and -7. The latter two data sets cover the entire area of interest for the 2013 winter season and the 2013-2014 summer season. The winter season data set has about 2400 samples while the summer season one about 1200.

4.1. VALIDATION OF THE PCL

4.1.1. Russian Site

The selected features for the iterative trimming are the sum, the mean, the range and the norm of the pixels' signal. A visual analysis revealed that the pre-seasonal cropland layer is spatially consistent to separate urban areas, forests and water. However, it appears that for some fragmented areas, e.g. small forest patches, the spatial resolution is insufficient. The field boundaries were converted to a raster; only pixels covering at least 50% of cropland were considered as such. The accuracy of the product was assessed thanks to the confusion matrix and the derived accuracy indices. The overall accuracy was 79%. Most errors are due to the fact that there is no natural vegetation class, therefore the cropland extent is overestimated (Fig. 11). One has to bear in mind that the reference used for the trimming is expected to improve as a high resolution reference would become available at the next of the season.
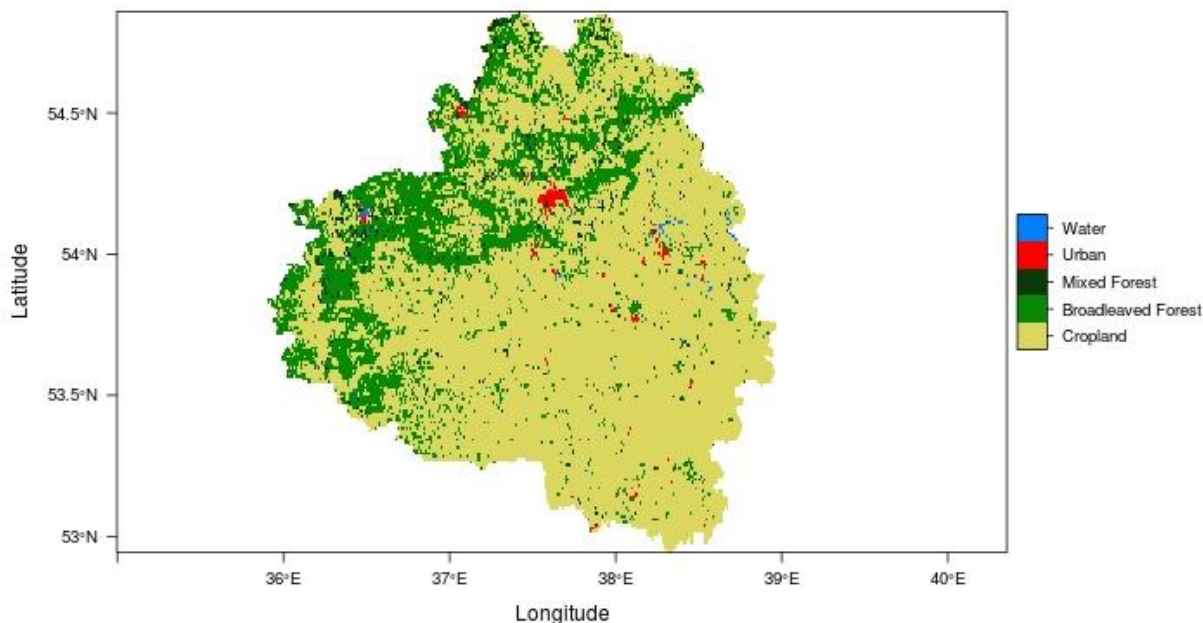
Figure 11: Result of the iterative trimming and the pre-seasonal cropland layer

4.1.2. South African site

The selected features for the iterative trimming are the sum, the max, the min and the maximum slope of the pixels' signal. A visual analysis revealed that the pre-seasonal cropland layer is spatially consistent to separate urban areas, forests and water (Fig. 12). However, it appears that for some areas mostly associated with less intensive cropping systems, the spatial resolution is insufficient. About ten thousand were extracted from the NLC2009 map and converted in two classes: cropland, non-cropland (Table 3). The accuracy of the product was assessed thanks to the confusion matrix and the derived accuracy indices. The overall accuracy was 76%; omission errors (43%) mostly occurred in less intensive areas.

Table 3: Confusion matrix for the pre-seasonal cropland layer -- Free State

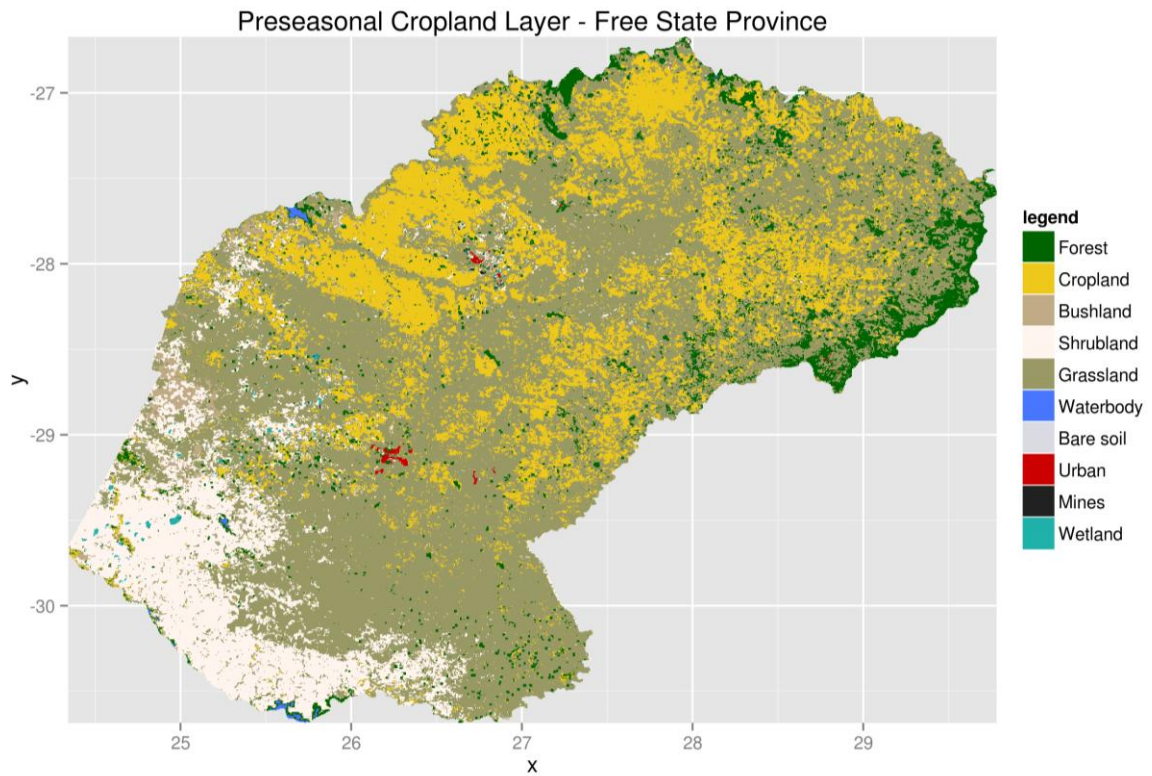| Map \ Reference	*Non Cropland*	*Cropland*	**Users' Accuracy**
Non cropland	626	125	83.4%
Cropland	80	169	67.9%
Producer's accuracy	88.7%	57.5%	Overall Accuracy: 75.9%

Figure 12: Pre-seasonal Cropland Layer - Free State Province

4.2. VALIDATION OF THE CGL

4.2.1. Russian Site

The algorithm described above was applied to produce the crop group layer of the growing season of 2013 (Fig. 13). Its accuracy was assessed and showed a global accuracy of 82% (Table 4). This level of accuracy is satisfactory considering the timing of this early estimation.
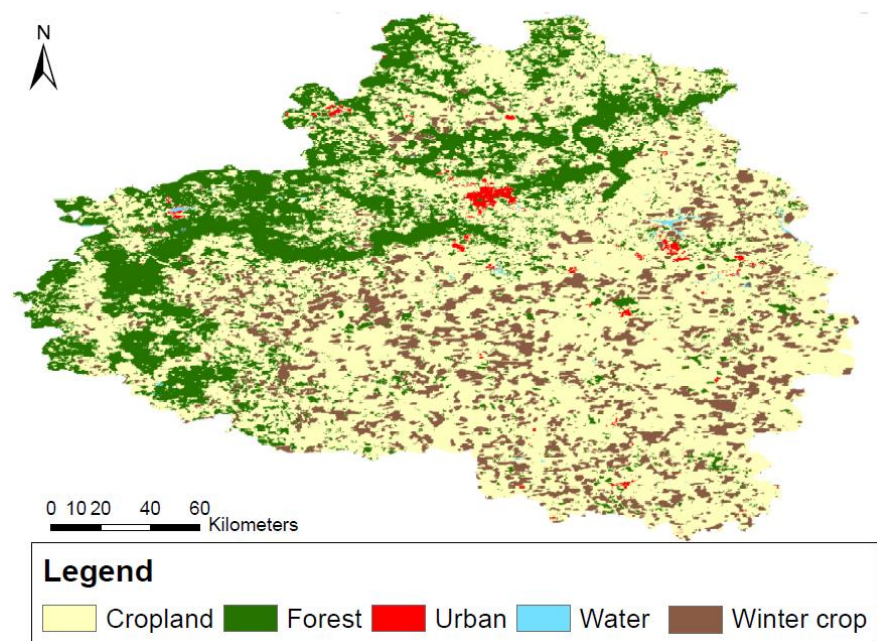

Figure 13: Crop group layer with land cover

Table 4: Confusion matrix for the crop group layer

Map \ Reference	*Other crops*	*Winter Wheat*	**User accuracy**
Other crops	348	74	82%
Winter crop	35	144	80%
Producer Accuracy	91%	66%	**Overall Accuracy**: 82%

For the winter crop class, one can observe an omission rate of 44% (100-Producer accuracy). This omission error was investigated thanks to the Pareto boundary (Boschetti, Flasse, & Brivio, 2004). At their early development stages, winter crops exhibit a large within field heterogeneity (Fig. 14). The error matrix does not consider contextual influence of mixed pixels on the product accuracy. The Pareto boundary method is an alternative to deal with these shortcomings. The number of low resolution pixels covering multiple classes is closely linked to the ground features (reference data) and is a function of their shape, size and spatial patterns. The difference in spatial resolution between high and low resolution data is referred to as the low-resolution bias. The resolution bias sets down the omission and commission errors as conflicting objectives: residual error after classification cannot be

avoided. Any attempt to reduce the commission errors will inevitably lead to an increase of the omission errors and conversely. A region of unreachable accuracy limited by the Pareto boundary because of the resolution bias decouples the errors due to the spatial resolution and the method. The Pareto boundary determines the maximum user and producer's accuracy values that could be attained jointly and represents such a lower limit as a boundary in the OE/CE bi-dimensional space. To generate the Pareto boundary, the high resolution reference map is degraded to the low resolution pixel size. Each new pixel value corresponds to the percentage of high resolution pixels of the class of interest. A set of low-resolution product is obtained by thresholding the low resolution reference map. For each threshold defining the percentage for which a pixel is considered as vegetation, the pair of efficient error rates OE/CE is computed. The line joining all these points defines the Pareto boundary of a specific high resolution reference to a defined low-resolution pixel size. Distance between the product and the boundary indicates the performance of the method.
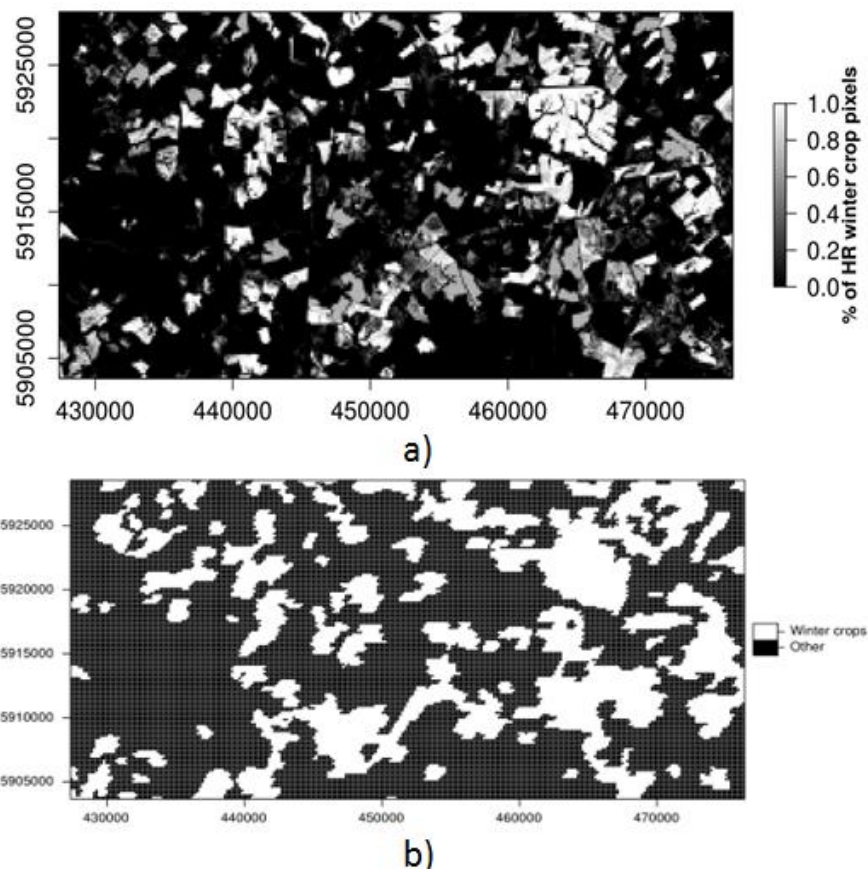

Figure 14: a) Reference winter crop map degraded at 250-m b) the corresponding crop group layer

First, the reference map was produced by classifying on a pixel basis two RapidEye images (Fig. 14) with an unsupervised clustering followed by a supervised labelling of the clusters. The resolution of the reference map was then degraded to the products. The pixel value corresponds to the percentage of high resolution winter crop pixels contained within it.

The Pareto boundary is above the 0.4 isoline which means that at this stage in the season a large part of the omission error is due to the spatial resolution (250-m) (Fig. 15).
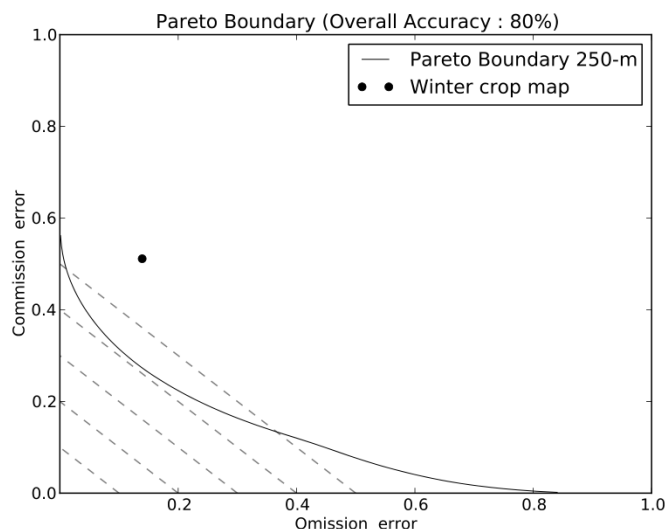

Figure 15: Pareto boundary for the winter crop class

4.2.2. South African site

The algorithm described above was applied to produce the crop group layer of the growing season of 2014 (Fig. 16). Its accuracy was assessed and showed a global accuracy of 97% (Table 5). The combination of RapidEye and Radarsat-2 data improved the field delineation and the spatial details at the cost of some commission, e.g. small tree lines.

Table 5: Confusion matrix for South Africa

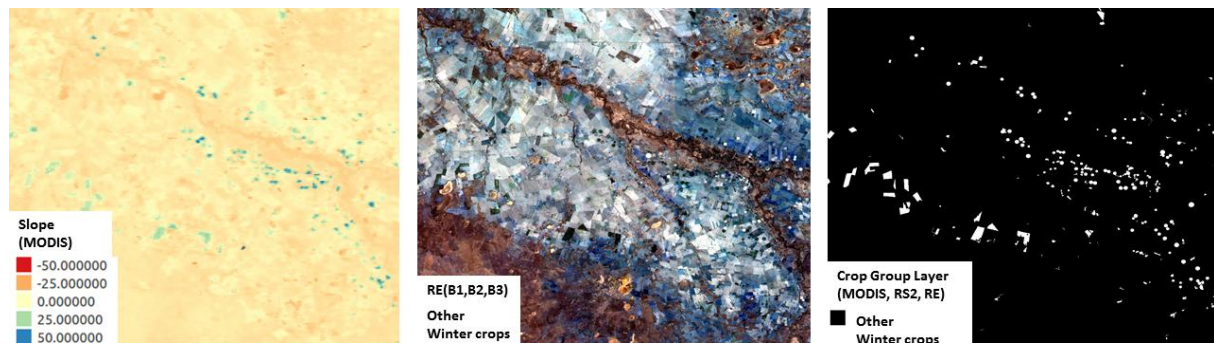| Map \ Reference	Other crops	Winter crops	Users' Accuracy
Other Crops	2171	29	98.7%
Winter Crops	80	169	68.9%
Producer's accuracy	97.8%	78.2%	Overall Accuracy: 96.8%

Figure 16: Successive improvements on the detection and delineation of winter crops

4.3. VALIDATION OF THE CTL

4.3.1. Russian Site

The CTL accuracy was tracked along the season; especially, the overall accuracy was chosen as indicator. Three different classifiers have been tested: the Naïve Bayes, the Support Vector Machine and the Random Forest. It was found that the Random Forest outperfomed the two others for every sensor and was therefore prefered (Fig. 17) and therefore was chosen to be implemented in the processing chains. Individually, the RapidEye-based classifcations meet the accuracy target (0.85) in mid-June. With the fused-maps (Fig. 18), the measured accuracy meets the target (0.85) also in mid-June (Fig. 19). The overall accuracy saturates then around 90% until the end of the season. The forest belt pattern is well captured and the resolution allows to map grassland accuracetly while it was not achievable with MODIS only.
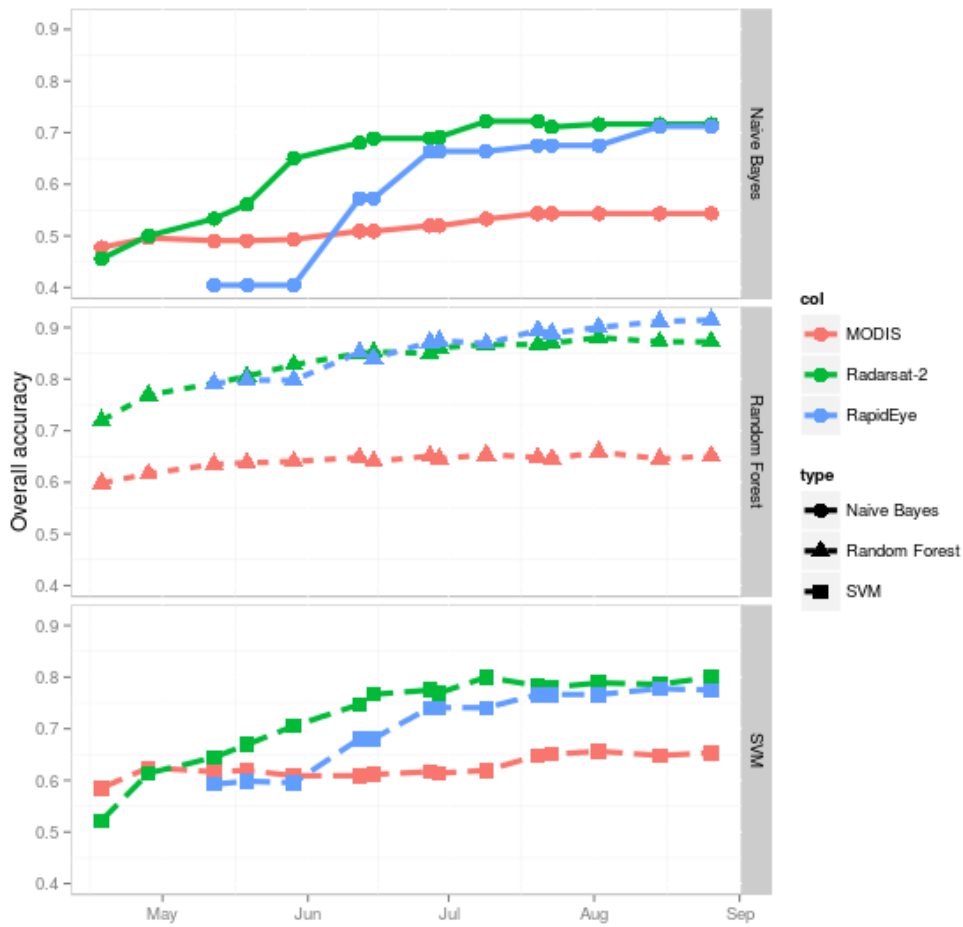
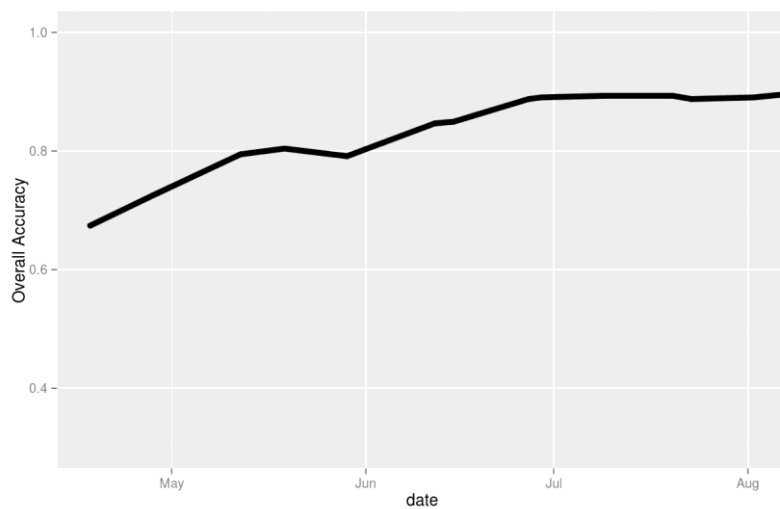**Figure 17: Evolution of the overall accuracy along the season by classifiers and by sensors**

Figure 18: Evolution of the overall accuracy for the fused map
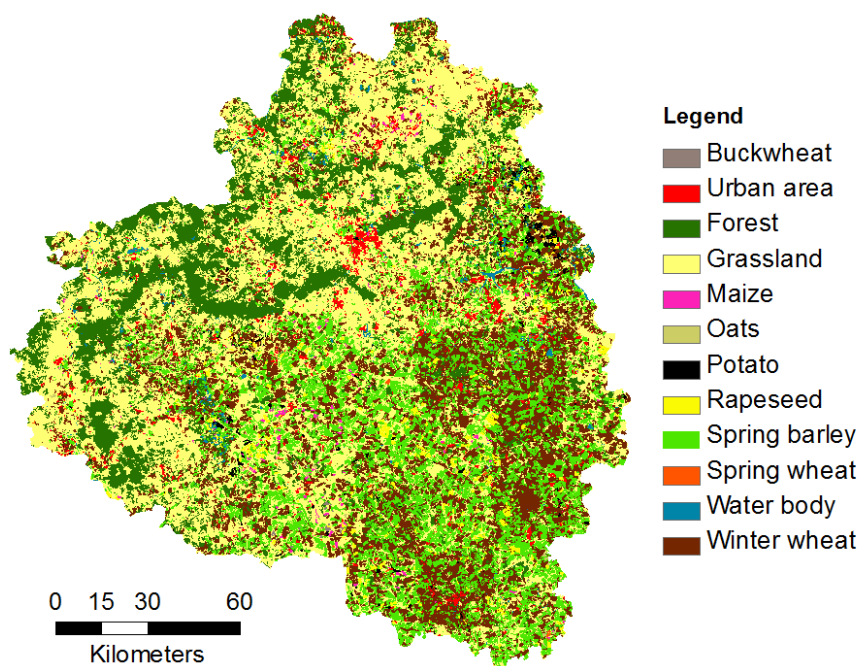
Figure 19: Crop Type Layer - Tula Oblast

4.3.2. South African site

The CTL for the Free State Province was validated with an independent set of about 1200 field observations. The overall accuracy reached a maximum of 78% at the end of the season (Figure 20). The maize and the planted pastures classes (the two most dominant classes) were the two classes with the highest accuracy (Fscore >0.8) (Figure 21).

Figure 20: Evolution of the Overall Accuracy along the season for different classes included in the CTL for the Free State Province

Figure 21: Evolution of the F-score along the season for different classes included in the CTL for the Free State Province

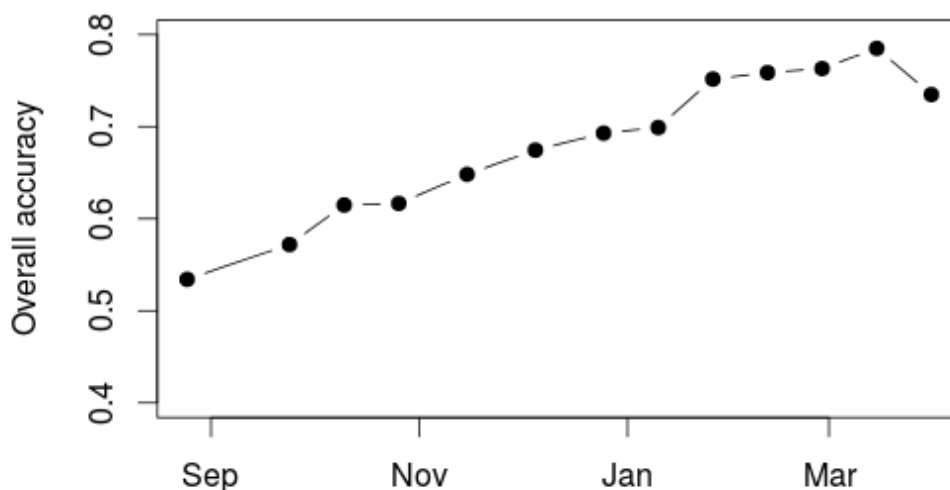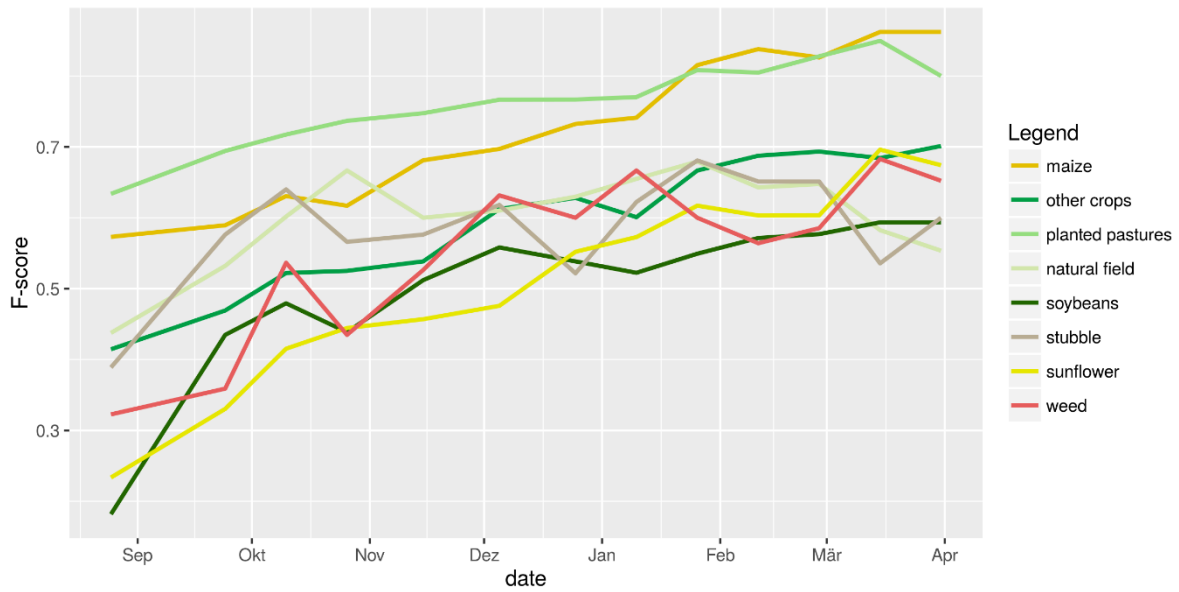The CTL allows identifying clear crop patterns such as an intensive maize area from Welkom to Bloemhof whereas the vicinity of Heilbron is dominated by soybean (Figure 22).
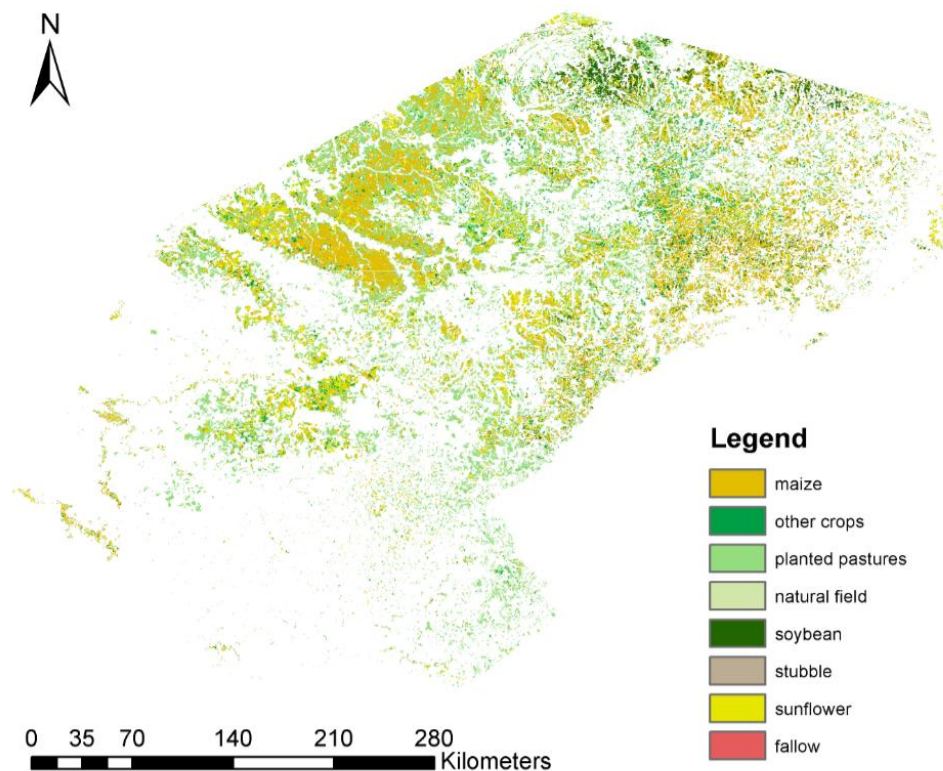
Figure 22: Crop Type Layer – Free State Province

4.4. LIMITS OF THE METHOD

The method proposed in this ATBD combines three different kinds of sensor and might be extended to more which reduces the sensor dependence and enhances the probability of acquiring during a good discrimination window. This combination makes the classification method more robust to address the large spectrum of agro-systems of the world.

Several peculiarities of the data sets used might introduce some limitations. First, the RapidEye imagery was at the top of canopy level. Because the acquisition window necessary to image the whole study of interest spanned on up to 20 days, differences in the atmospheric conditions are more than likely. Second, clouds were masked using the default RapidEye quality flag which tends to be affected by omission errors. Third, due to the large acquisition windows, difference in vegetation stages may have occurred throughout the area of interest which complicates the recognition process. These factors constrain particularly the reachable accuracy when mapping large areas as crop practices, climate gradient and landscape properties are likely to be heterogeneous. As an example, the Free State Province is characterized by a strong longitudinal gradient in meteorological conditions as well as in planting density. In addition, the planting window for maize stretches on several months. All

together, these factors lead to natural diversity of maize spectral-temporal signature. The additional variability resulting from the data set itself, may explain why the Fscore of certain crop types did not exceed 0.7. Effects of the between tile variability are especially visible at the beginning of the season.

Regarding the pre-seasonal cropland layer, the reference has to be of reasonable accuracy in order to produce accurate results. Indeed, if a class is dominated by mislabeled pixels, the trimming would tend to remove the correctly labeled data because of the spectral distribution shift introduced by the mislabeled pixels. Besides, other features might appear more relevant in other agro-systems and could easily replace the four proposed here. In the case of high cloud coverage during the winter, the identification of the winter growth peak might be less accurate leading to more confusion between winter crops and summer crops. In the full-season case, defining the parameters for the segmentations and the number of clusters for the multi-source crop group recognition would need some fine tuning to be adapted on a new site. Finally for the machine learning step, texture, vegetation indices, temporal features might be considered to increase the accuracy of the recognition. The main constraint is the availability of training data. Strategies can be set up to provide such data sets without sending teams for in-situ data collection such as working with the time-series of the previous year, dynamic time warping to identify likely trajectories (Petitjean et al., 2012) expected trajectories (growing degree days), crop calendars, decision rules, crowd-sourcing and kriging (Masse, 2013). To ensure that the approach presented in this ATBD is applicable in the absence of within season calibration/validation data –which would be the case when running the algorithm along the season in near real time– the fusion of the maps coming from different sensors does not rely on field data. In case such data become available, one could use them to weight the class membership according to class-wise accuracies of the maps.

5. CONCLUSION AND PERSPECTIVE

The pre-seasonal cropland layer, the crop group layer and the crop type layer capitalize on the synergy of Sentinel-1, Sentinel-2 and Sentinel-3 like images to monitor continuously the cropland status along the growing season. The products provide consistent maps with an increasing level of thematic and spatial details as information accumulates and exceed the accuracy target of 85%. The classification system was designed to reduce the dependence to a specific data source which is desired for operational monitoring. Beside, emphasis was put on the portability of the method.

6. REFERENCES

Ainsworth, T.L., J. P. Kelly, and J. Lee, "Comparisons between dual-pol, compact polarimetric and quad-pol SAR imagery," ISPRS J. Photogramm. Remote Sens., vol. 64, no. 5, pp. 464–471, Sep. 2009.

Arvor, Damien, Johnathan, Milton, Meirelles, Margareth Simões Penello, et al. Classification of MODIS EVI time series for crop mapping in the state of Mato Grosso, Brazil. International Journal of Remote Sensing, 2011, vol. 32, no 22, p. 7847-7871

Atzberger, Clement and Rembold, Felix. Portability of neural nets modeling regional winter crop acreages using AVHRR time series. Eur. J. Remote Sens, 2012, vol. 45, p. 371-392.

Baatz, M. and A. Schape (2000). Multiresolution Segmentation - An Optimization Approach for High Quality Multi-Scale Image Segmentation. Angewandte Geographische Informations verarbeitung XII, Ed. J Strobl et al. AGIT Symposium, Salzburg, Germany, 2000. pp. 12-23.

Bartholomé, E. M. and Belward A. S., 2005, GLC2000; a new approach to global land cover mapping from Earth Observation data, International Journal of Remote Sensing, 26, 1959 – 1977

Biradar, C.M.; Thenkabail, P.S.; Noojipady, P.; Li, Y.; Dheeravath, V.; Turral, H.; Velpuri, M.; Gumma, M.K.; Gangalakunta, O.R.P. ; Cai, X.L.; et al. A global map of rainfed cropland areas (GMRCA) at the end of last millennium using remote sensing. Int. J. Appl. Earth Obs. Geoinf. 2009, 11, 114–129.

Blaes,X, L. Vanhalle, and P Defourny. Efficiency of crop identification based on optical and SAR image time series. Remote Sensing of Environment, 96(3-4):352–365, 2005.

Bontemps, S., Defourny, P., Brockmann, C., Herold, M., Kalogirou, V., Arino, O. 2012, New Global Land Cover mapping exercise in the framework of the ESA Climate Change Initiative, Proceedings IEEE International Geoscience and Remote Sensing Symposium (IGARSS)

Bontemps S., Van Bogaert E., Defourny P., Kalogirou V. and Arino O., GlobCover 2009, "Products description manual", December 2010.

Boschetti, L., Flasse, S., & Brivio, P. (2004). Analysis of the conflict between omission and commission in low spatial resolution dichotomic thematic products: The Pareto Boundary. *Remote Sensing of Environment*, 91(3-4):280–292.

Breiman, L. (2001). Random forests. *Machine learning*, 45(1), 5-32.

Bruzzone, L., Roli, F., & Serpico, S. B. (1995). An extension of the Jeffreys-Matusita distance to multiclass cases for feature selection. *IEEE Transactions on Geoscience and Remote Sensing*, 33(6), 1318-1321.

Castillejo-Gonzalez, Isabel Luisa, Lopez-Granados, Francisca, Garcia-Ferrer, Alfonso, et al. Object-and pixel-based analysis for mapping crops and their agro-environmental associated measures using QuickBird imagery. Computers and Electronics in Agriculture, 2009, vol. 68, no 2, p. 207-215.

Chen, C. and K. Chen, "The use of fully polarimetric information for the fuzzy neural classification of SAR images," IEEE Trans. Geosci. Remote Sens., vol. 41, no. 9, pp. 2089–2100, Sep. 2003.

Cloude, S.R., and E. Pottier, "A review of target decomposition theorems in radar polarimetry," IEEE Trans. Geosci. Remote Sens., vol. 34, no. 2, pp. 498–518, Mar. 1996.

Desclée, B., Bogaert, P., & Defourny, P. (2006). Forest change detection by statistical object-based method. *Remote Sensing of Environment*, 102(1-2):1–11.

Del Frate, F., G. Schiavon, D. Solimini, M. Borgeaud, D. H. Hoekman, and M. A. M. Vissers, "Crop classification using multiconfiguration C-band SAR data," IEEE Trans. Geosci. Remote Sens., vol. 41, no. 7, pp. 1611–1619, Jul. 2003.

Defourny, P., Bicheron, P., Brockmann, C., Bontemps, S., Van Bogaert, E., Vancutsem, C., Huc, M., Leroy, M., Ranera, F., Achard, F., Di Gregorio, A., Herold, M., and Arino, O., 2009. The first 300-m Global Land Cover Map for 2005 using ENVISAT MERIS time series: a Product of the GlobCover System. In: Proceedings of the 33rd International Symposium on Remote Sensing of Environment (ISRSE). Stresa, Italy.

Delrue, Josefien, Byderkerke, Lieven, Eerens, Herman, et al. Crop mapping in countries with small-scale farming: a case study for West Shewa, Ethiopia. International Journal of Remote Sensing, 2013, vol. 34, no 7, p. 2566-2582.

De Wit, A. J., & Clevers, J. G. (2004). Efficiency and accuracy of per-field classification for operational crop mapping. *International Journal of Remote Sensing*, 25(20):4091–4112.

Eilers, P. H. (2003). A Perfect Smoother. *Analytical Chemistry* , 75(14):3631–3636.

Friedl, M.A.; Mciver, D.K.; Hodges, J.C.F.; Zhang, X.Y.; Muchoney, D.; Strahler, A.H.; Woodcock, C.E.; opal, S.; Schneider, A.; Cooper, A.; et al. Global land cover mapping from MODIS: Algorithms and early results. Remote Sens. Environ. 2002, 83, 287–302.

Fritz, S.; You, L.; Bun, A.; See, L.; McCallum, I.; Schill, C.; Perger, C.; Liu, J.; Hansen, M.; Obersteiner, M. Cropland for sub-Saharan Africa: A synergistic approach using five land cover data sets. Geophys. Res. Lett. 2011, doi:10.1029/2010GL046213.

Hänsch, R.,"Complex-valued multi-layer perceptrons—An application to polarimetric SAR data," Photogram. Eng. Remote Sens., vol. 76, no. 9, pp. 1081–1088, Sep. 2010.

Jakubauskas, M., Legates, D., & Kastens, J. (2002). Crop identification using harmonic analysis of time-series AVHRR NDVI data. *Computers and Electronics in Agriculture*, 37(1-3):127–139.

Kastens J., T Kastens, D Kastens, K Price, E Martinko, and R Lee. Image masking for crop yield forecasting using AVHRR NDVI time series imagery. Remote Sensing of Environment, 99(3):341–356, November 2005

Hégarat-Mascle, S. L., Richard, D., & Ottlé, C. (2003). Multi-scale data fusion using Dempster-Shafer evidence theory. *Integrated Computer-Aided Engineering*, 10(1), 9-22.

Lee, J.S., M. R. Grunes, and E. Pottier, "Quantitative comparison of classification capability: Fully polarimetric versus dual and single-polarization SAR," IEEE Trans. Geosci. Remote Sens., vol. 39, no. 11, pp. 2343–2351, Nov. 2001.

Lobell, D.B. Asner, G.P. Cropland distributions from temporal unmixing of MODIS data. Remote Sens. Environ. 2004, 93, 412–422.

McNairn, H., Catherine Champagne, Jiali Shang, Delmar Holmstrom, and Gordon Reichert. Integration of optical and Synthetic Aperture Radar (SAR) imagery for delivering operational annual crop inventories. ISPRS Journal of Photogrammetry and Remote Sensing, 64(5):434–449, September 2009.

Masse, A., Development and automation of classification methods from remote sensing image time series- Application to land use changes and carbon footprint estimation, 2013, Université Toulouse III Paul Sabatier

Mayaux, P.; Bartholome, E.; Fritz, S.; Belward, A. A new land-cover map of Africa for the year 2000. J. Biogeogr. 2004, 31, 861–877

Ok, Asli Ozdarici, Akar, Ozlem, et Gungor, Oguz. Evaluation of random forest method for agricultural crop classification. European Journal of Remote Sensing, 2012, vol. 45, p. 421-432.

Ormeci, Cankut, Alganci, Ugur, et Sertel, Elif. Identification of Crop Areas Using SPOT–5 Data. In : Proceedings of the FIG Congress. 2010.

Ozdogan, Mutlu. The spatial distribution of crop types from MODIS data: temporal unmixing using independent component analysis. Remote Sensing of Environment, 2010, vol. 114, no 6, p. 1190-1204.

Petitjean, F., Inglada, J., Gancarski, P., 'Satellite Image Time Series Analysis Under Time Warping' IEEE Transactions on Geoscience and Remote Sensing, 2012, Vol.50-8, pp.3081-3095

Pittman, K.; Hansen, M.C.; Becker-Reshef, I.; Potapov, P.V.; Justice, C.O. Estimating global cropland extent with multi-year MODIS data. Remote Sens. 2010, 2, 1844–1863.

Portmann, F.T.; Siebert, S.; Doll, P. MIRCA2000—Global monthly irrigated and rainfed crop areas around the year 2000: A new high-resolution data set for agricultural and hydrological modeling. Glob. Biogeochem. Cy. 2010, doi:10.1029/2008GB003435.

Qi, J., Chehbouni, A., Huete, R., & Kerr, Y. a. (1994). A modified soil adjusted vegetation index. *Remote Sensing of Environment*, 48(2):119–126.

Radoux, J. (2010). Updating land cover maps by GIS-driven analysis of very high resolution satellite images. *PhD Thesis, Université catholique de Louvain*.

Ramankutty, N.; Evan, A.; Monfreda, C.; Foley, J.A. Farming the planet. Part 1: The geographic distribution of global agricultural lands in the year 2000. Glob. Biogeochem. Cy. 2008, doi:10.1029/2007GB002952.

Shao, Yang, Lunetta, Ross S., Ediriwickrema, Jayantha, et al. Mapping cropland and major crop types across the Great Lakes Basin using MODIS-NDVI data. Photogrammetric engineering and remote sensing, 2010, vol. 76, no 1, p. 73-84.

Skriver, H., F. Mattia, G. Satalino, A. Balenzano, V. R. N. Pauwels, N. E. C. Verhoest, and M. Davidson, Crop classification using short-revisit multitemporal SAR data," IEEE J. Sel. Topics Appl. Earth Observat. Remote Sens., vol. 4, no. 2, pp. 423–431, Jun. 2011.

Thenkabail, P.S.; Wu, Z. An Automated Cropland Classification Algorithm (ACCA) for Tajikistan by Combining Landsat, MODIS, and Secondary Data. Remote Sens. 2012, 4, 2890-2918

Thenkabail, P.S.; Biradar, C.M.; Noojipady, P.; Dheeravath, V.; Li, Y.J.; Velpuri, M.; Gumma, M.; Reddy, G.P.O. Turral, H.; Cai, X.L. A Global irrigated area map (GIAM) using remote sensing at the end of the last millennium. Int. J. Remote Sens. 2009, 30, 3679–3733.

Uhlmann, S. and Kiranyaz, S.; Integrating Color Features in Polarimetric SAR Image Classification, IEEE Transactions on Geoscience and Remote Sensing, Vol. 52, N.4,pp. 2197- 2216, 2014

Vancutsem, C.; Marinho, E.; Kayitakire, F.; See, L.; Fritz, S. Harmonizing and Combining Existing Land Cover/Land Use Datasets for Cropland Area Monitoring at the African Continental Scale. Remote Sens. 2013, 5, 19-41

Vancutsem, C. ,.-F. (2007). Mean compositing, an alternative strategy for producing temporal syntheses: Concepts and performance assessment for SPOT VEGETATION time-series. *International Journal of Remote Sensing*, 28:5123–5141.

Vintrou, Elodie, Desbrosse, Annie, B égué, Agnès, et al. Crop area mapping in West Africa using landscape stratification of MODIS time series and comparison with existing global land products. International Journal of   Applied Earth Observation and Geoinformation, 2012, vol. 14, no 1, p. 83-93.

Yang, Chenghai, Everitt, James H., Fletcher, Reginald S., et al. Using high resolution QuickBird imagery for crop identification and area estimation.Geocarto International, 2007, vol. 22, no 3, p. 219-233.

Yang, W., D. Dai, J. Wu, and C. He, "Weakly supervised polarimetric SAR image classification with multi-modal Markov aspect model," in Proc. TC 7th Symp. 100 Years ISPRS, vol. 38. Vienna, Austria, Jul. 2010, pp. 5–9.